Spiral ground state in the quasi-two-dimensional spin-$\frac{1}{2}$ system Cu_2GeO_4

Alexander A. Tsirlin,[1,*] Ronald Zinke,[2] Johannes Richter,[2] and Helge Rosner[1,†]
[1]*Max Planck Institute for Chemical Physics of Solids, Nöthnitzer Strasse 40, D-01187 Dresden, Germany*
[2]*Institute for Theoretical Physics, University of Magdeburg, P.O. Box 4120, D-39016 Magdeburg, Germany*
(Received 20 August 2010; revised manuscript received 1 October 2010; published 22 March 2011)

We apply density functional theory band structure calculations, the coupled cluster method, and exact diagonalization to investigate the microscopic magnetic model of the spin-$\frac{1}{2}$ compound Cu_2GeO_4. The model is quasi-two-dimensional, with uniform spin chains along one direction and frustrated spin chains along the other direction. The coupling along the uniform chains is antiferromagnetic, $J \simeq 130$ K. The couplings along the frustrated chains are $J_1 \simeq -60$ K and $J_2 \simeq 80$ K between nearest neighbors and next-nearest neighbors, respectively. The ground state of the quantum model is a spiral, with a reduced sublattice magnetization of 0.62 μ_B and a pitch angle of 84°, both renormalized by quantum effects. The proposed spiral ground state of Cu_2GeO_4 opens a way to magnetoelectric effects in this compound.

DOI: 10.1103/PhysRevB.83.104415 PACS number(s): 75.30.Et, 75.10.Jm, 71.20.Ps, 75.50.Ee

I. INTRODUCTION

Quantum magnetism is a field of fundamental research focused on exotic ground states and nontrivial low-temperature properties.[1,2] Nevertheless, certain effects in quantum magnets are also relevant for applications. Spin-chain compounds show a ballistic regime of heat transport,[3] whereas frustrated magnets are capable of a strong magnetocaloric effect.[4,5] Additionally, many of the frustrated magnets undergo spiral or, in general, incommensurate ordering and reveal ferroelectricity induced by a magnetic field.[6] A frustrated spin chain with competing ferromagnetic (FM) nearest-neighbor (J_1) and antiferromagnetic (AFM) next-nearest-neighbor (J_2) couplings is the simplest spin model giving rise to spiral magnetic correlations at $J_2/J_1 < -\frac{1}{4}$ (Ref. 7). This model is easily realized experimentally and has a clear structural footprint, a chain of edge-sharing CuX_4 plaquettes with X being oxygen,[8–11] chlorine,[12] or even nitrogen.[13] Such chains typically show FM J_1 due to the nearly 90° Cu-X-Cu angle and AFM J_2 due to the Cu-X-X-Cu superexchange. Indeed, many compounds of this type undergo spiral magnetic ordering and sometimes exhibit magnetic field-induced ferroelectricity.[14] However, the detailed microscopic understanding of these effects remains challenging, and even the electronic origin of ferroelectricity in spin-chain cuprates is vividly debated.[15]

Interchain couplings are an important feature of any real material. The couplings between spin chains can modify the ground state qualitatively by inducing a long-range order with finite sublattice magnetization.[16,17] In the case of frustrated spin chains, such couplings influence the behavior of doped systems[18] and play a decisive role for the stability of exotic phases in high magnetic fields.[19,20] Regarding magnetoelectric effects, the interchain couplings naturally determine their temperature scale by adjusting the magnetic ordering temperature.

Theoretical studies of coupled frustrated spin chains remain a challenge owing to the two-dimensional (2D) and frustrated nature of the problem. Therefore, experimental benchmarks are especially important. The available frustrated-spin-chain compounds show relatively weak interchain couplings,[20] while the relevance of the opposite regime with strongly coupled frustrated spin chains remains unclear. A common and a somewhat naive picture suggests that leading exchange couplings should run along the structural chains owing to shorter Cu-Cu distances.[21]

In the following, we present a microscopic magnetic model of Cu_2GeO_4. This compound is a unique example of a 2D system of strongly coupled frustrated spin chains. The coupling J between the frustrated chains is so strong that the system can be equally viewed as uniform spin chains along J with the frustrated interchain couplings J_1 and J_2 (see Fig. 1). Both descriptions relate to certain features of the magnetic behavior: while the uniform chain model fits the magnetic susceptibility of Cu_2GeO_4 down to $T/J \simeq 0.5$, the ground state of the 2D model is a spiral, which is typical for the frustrated J_1-J_2 spin chains.

The crystal structure of Cu_2GeO_4 belongs to the spinel type.[22] Magnetic properties were studied in a relation to the spin-Peierls compound $CuGeO_3$. The low-dimensional magnetic behavior of Cu_2GeO_4 resembles $CuGeO_3$ indeed. However, no signatures of the structural distortion or spin gap were found down to 10 K, and the long-range magnetic ordering at $T_N = 33.1$ K is observed instead.[23]

Yamada *et al.*[23] analyzed Cu_2GeO_4 using the anisotropic pyrochlore lattice model with two inequivalent exchange couplings that are J_1 and J_c in our notation (upper left panel of Fig. 1). This model arises from a straightforward and naive geometrical consideration of the spinel structure, with inequivalent couplings driven by the tetragonal distortion of the parent cubic system. At $J_c/J_1 \ll 1$, the anisotropic pyrochlore lattice splits into chains. According to Ref. 23, Cu_2GeO_4 is close to this limit, with $J_1 = 135$ K and $J_c/J_1 = 0.16$. Starykh *et al.*[24] studied the 2D analog of the model theoretically and proposed a quantum-disordered valence-bond-solid ground state.

II. BAND STRUCTURE

As a derivative of the spinel structure, Cu_2GeO_4 might be thought of as a three-dimensional network of CuO_6 octahedra. However, this description ignores essential features of the electronic structure. In oxide compounds, Cu^{2+} tends to adopt a fourfold coordination (CuO_4 plaquette) having dramatic influence on the orbital ground state and magnetic properties. Such plaquettes can be recognized in Cu_2GeO_4 and lead to a

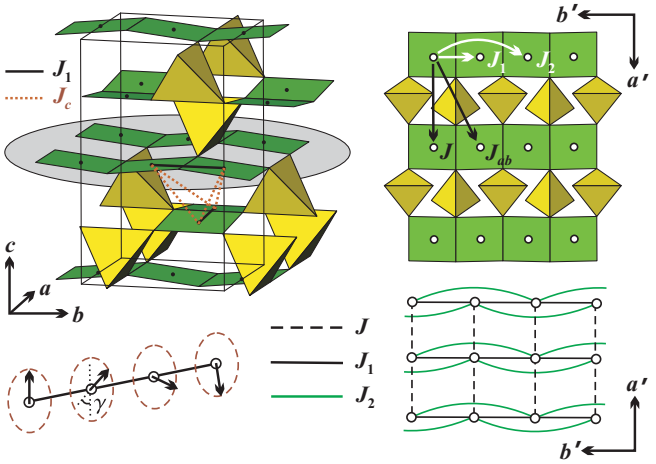

FIG. 1. (Color online) Top panel: Crystal structure of Cu_2GeO_4 (left) and a single magnetic layer in the ab plane (right). Bottom panel: A sketch of the spin spiral with the pitch angle γ (left) and the magnetic model of J_1-J_2 frustrated spin chains coupled by J (right). Circles and dots denote the positions of the Cu atoms. Lines in the top left panel show the anisotropic pyrochlore lattice considered in Ref. 23.

peculiar superexchange scenario. Four short bonds to oxygen (1.95 Å) form the CuO_4 plaquettes in the ab plane, whereas the two remaining Cu-O bonds are much longer (2.50 Å). Edge-sharing CuO_4 plaquettes comprise structural chains that run along a or b, with parallel chains forming layers in the ab plane (upper right panel of Fig. 1). Equivalent layers with differently directed structural chains alternate along the c axis. In the following, we denote the direction of the structural chains as b' and the perpendicular direction as a', to distinguish those from the crystallographic a and b axes. GeO_4 tetrahedra connect the chains into a three-dimensional (3D) framework (Fig. 1).

To evaluate individual exchange couplings, we perform scalar-relativistic density functional theory (DFT) band structure calculations using the FPLO9.00-33 code.[25] We apply the local density approximation (LDA) with the exchange-correlation potential by Perdew and Wang[26] and use a well-converged k mesh comprising 3350 points in the symmetry-irreducible part of the first Brillouin zone. With LDA calculations, we are able to identify relevant states and to evaluate hopping parameters t_i via a fit with an effective one-orbital tight-binding (TB) model. The hopping parameters are introduced into a Hubbard model with the effective on-site Coulomb repulsion potential $U_{\rm eff} = 4.5$ eV.[27–29] In the case of low-lying excitations, the Hubbard model is further reduced to a Heisenberg model under the conditions of half-filling and strong correlations ($t_i \ll U_{\rm eff}$). Then, the AFM parts of the exchange integrals are evaluated as $J_i^{\rm AFM} = 4t_i^2/U_{\rm eff}$.

An alternative way to evaluate the exchange couplings is to treat the strong correlations within DFT, via the mean-field-like LSDA + U approach. We calculate total energies for a set of collinear spin configurations and map these energies onto a classical Heisenberg model. Thus, total exchange integrals J_i are estimated. In the LSDA + U calculations, we use the Coulomb repulsion and exchange parameters $U_d = 6.5 \pm 1$ eV and

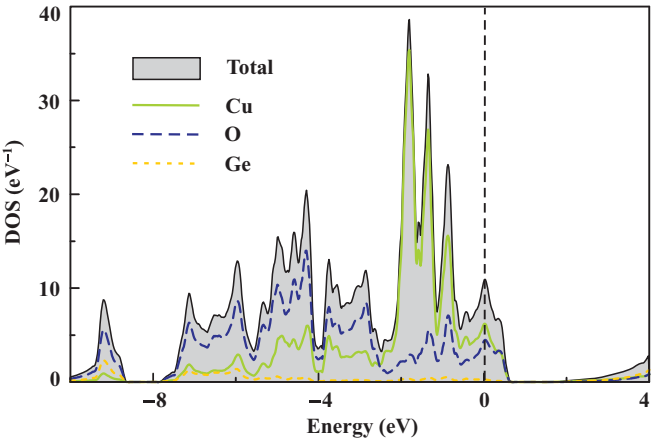

FIG. 2. (Color online) LDA density of states for Cu_2GeO_4. The Fermi level is at zero energy.

$J_d = 1$ eV, respectively.[28–30] The double-counting-correction (DCC) scheme was set to the around-mean-field (AMF) option. The application of the fully-localized-limit (FLL) DCC had little effect on the exchange couplings.

The LDA energy spectrum of Cu_2GeO_4 is typical for Cu^{+2} oxides. The mixed Cu $3d$-O $2p$ valence bands extend down to −8 eV (Fig. 2), with the states near the Fermi level predominantly formed by the Cu $d_{x^2-y^2}$ orbital (here, x and y align with the short Cu-O bonds). Germanium orbitals contribute to the bands around −10 eV and show negligible DOS at higher energies. While LDA yields a metallic energy spectrum due to the underestimation of electronic correlations in the Cu $3d$ shell, LSDA + U restores the insulating scenario with the band gap of $E_g = 2.0 \pm 0.3$ eV for $U_d = 6.5 \pm 1$ eV.

The Cu $d_{x^2-y^2}$ states are represented by four bands crossing the Fermi level and arising from four Cu atoms in the primitive cell of Cu_2GeO_4 (Fig. 3). These bands are separated from the rest of the valence bands by a pseudogap. To extract hopping parameters, we construct Wannier functions (WFs) based on the Cu $d_{x^2-y^2}$ character.[31] This analysis evidences sizable nearest-neighbor (t_1) and next-nearest-neighbor (t_2) hoppings along the structural chains. However, the hopping

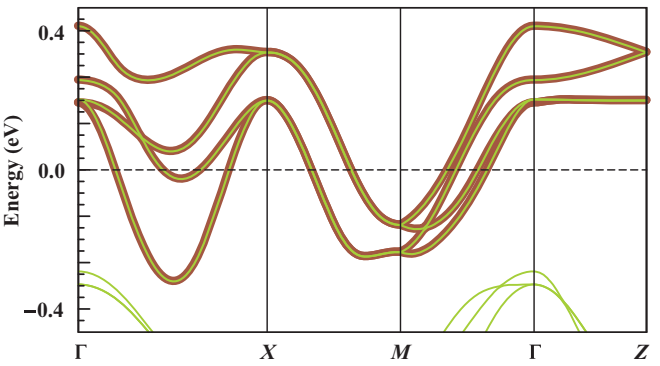

FIG. 3. (Color online) LDA band structure of Cu_2GeO_4 (thin light lines) and the fit of the TB model (thick dark lines). The Fermi level is at zero energy. The k path is defined as follows: $\Gamma(0,0,0)$, $X(0.5,0,0)$, $M(0.25,0.25,0)$, and $Z(0,0,0.5)$, where the coordinates are given in units of the reciprocal lattice parameters $4\pi/a$ and $4\pi/c$.

TABLE I. Leading exchange couplings in Cu_2GeO_4: hopping parameters t_i of the TB model, AFM contributions to the exchange couplings $J_i^{\rm AFM} = 4t_i^2/U_{\rm eff}$, and the total exchange integrals J_i from LSDA + U calculations with $U_d = 6.5$ eV.

	Cu-Cu distance (Å)	t_i (meV)	$J_i^{\rm AFM}$ (K)	J_i (K)
J_1	2.80	118	144	−60
J_2	5.59	82	70	80
J	5.59	115	137	130
J_{ab}	6.25	−37	14	7
J_c	3.07	−11	1	−2

t along a' is comparable to t_1 and t_2. Additionally, a weak diagonal hopping in the ab plane is found (Table I). The nearest-neighbor hoppings perpendicular to the ab plane (t_c) are −11 meV, yielding $J_c^{\rm AFM}$ as low as 1 K. The weak dispersion of the bands along Γ-Z also shows the pronounced two-dimensionality of the system. Introducing the hoppings into an effective one-band Hubbard model, we evaluate AFM parts of the exchange integrals $J_i^{\rm AFM}$ (Table I).

LSDA + U calculations modify the LDA-based scenario. We find FM nearest-neighbor coupling within the structural chains, $J_1 = -60 \mp 10$ K for $U_d = 6.5 \pm 1$ eV. The next-nearest-neighbor intrachain coupling $J_2 = 80 \mp 20$ K and the interchain coupling $J = 130 \mp 30$ K are basically unchanged. Further couplings in the ab plane are below 10 K. The interplane coupling becomes FM and remains weak. Thus, we establish the quasi-2D J-J_1-J_2 model with a weak interlayer coupling J_c (Fig. 1).

The quasi-2D model of Cu_2GeO_4 results from the strong tetragonal distortion of the spinel structure. The plaquette description (Fig. 1), with the magnetic $d_{x^2-y^2}$ orbital coplanar to the CuO_4 plaquette, clarifies the 2D nature of the system. The couplings J_c connect the plaquettes lying in different planes and therefore remain weak. By contrast, three sizable couplings in the ab plane establish a frustrated spin lattice. Our model is dissimilar to the anisotropic pyrochlore lattice proposed by Yamada *et al.*[23] The pyrochlore spin lattice omits the relevant exchanges J and J_2, and should be discarded. Cu_2GeO_4 is a frustrated magnet indeed, but the strong frustration is found in the J_1-J_2 chains rather than in the tetrahedral units.

The FM nearest-neighbor coupling J_1 should be referred to the Cu-O-Cu angle of 91.8°. The microscopic origin of ferromagnetism is the Hund's coupling on the oxygen site.[8] The next-nearest-neighbor coupling J_2 is the AFM Cu-O-O-Cu superexchange. Similar values of 50–100 K for $|J_1|$ and J_2 have been established for the archetype frustrated-spin-chain compounds, such as $LiCu_2O_2$ and $LiCuVO_4$.[8,10]

Another remark on the structural implementation of the spin model regards the origin of the long-range couplings J and J_2. Since the Ge orbitals weakly contribute to the valence states, both couplings should be assigned to a Cu-O-O-Cu superexchange. Despite an identical Cu-Cu distance (Table I), a larger J value is caused by the coplanar arrangement of the plaquettes in the adjacent chains. By contrast, the next-nearest-neighbor plaquettes within the chain (J_2) lie in different planes due to the buckled chain geometry (Fig. 1). It is worth noting that the ab projections of the Cu_2GeO_4 and $LiCuVO_4$ structures are very similar. However, $LiCuVO_4$ is a quasi-1D system with $J \ll |J_1|, J_2$, while the spin system of Cu_2GeO_4 is quasi-2D.[10]

III. MICROSCOPIC MODEL

In the following, we explore the ground state and finite-temperature properties of our model. We first consider the purely 2D regime described by the Hamiltonian

$$H = \sum_n \left\{ \sum_i [J_1\, \mathbf{s}_{i,n} \cdot \mathbf{s}_{i+1,n} + J_2\, \mathbf{s}_{i,n} \cdot \mathbf{s}_{i+2,n}] \right\} + \sum_i \sum_n J\, \mathbf{s}_{i,n} \cdot \mathbf{s}_{i,n+1}, \quad (1)$$

where the index n labels the structural chains (along b') and i denotes the lattice sites within a chain n. The effect of the interlayer coupling J_c is discussed in Sec. III D.

Our model can be viewed as frustrated J_1-J_2 chains (along b') which are uniformly coupled by J (along a'). Alternatively, one finds uniform spin chains along a' with frustrated interchain couplings J_1 and J_2 along b'. While any of the parent 1D models is rather easy to handle, a rigorous treatment of their 2D combination is a challenging problem. Below, we apply the Lanczos diagonalization and the coupled cluster method to achieve an accurate description of the ground state. By contrast, finite-temperature properties of the quantum model can only be accessed at high temperatures by a series expansion (HTSE), whereas conventional techniques, such as quantum Monte Carlo or exact diagonalization, fail because of the sign problem or finite-size effects.[32]

A. Magnetic susceptibility

Since the experimental information on Cu_2GeO_4 is restricted to the magnetic susceptibility and heat capacity measurements in Ref. 23, we discuss thermodynamic properties first. The experimental specific heat contains an unknown phonon contribution; hence the magnetic part cannot be separated. Therefore, the magnetic susceptibility $\chi(T)$ (Fig. 4) remains the only quantity suitable for the comparison between theory and experiment. The estimated Curie-Weiss temperature $\theta \simeq \frac{1}{2}(J + J_1 + J_2) = 75$ K is in good agreement with the experimental value of $\theta = 89$ K.[23]

For a further comparison, we derive the HTSE for our model:

$$\chi = \frac{N_A g^2 \mu_B^2}{4 k_B T} \left(1 + \frac{J + J_1 + J_2}{2T} + \frac{J^2 + J_1^2 + J_2^2}{4T^2} \right)^{-1}, \quad (2)$$

where N_A is Avogadro's number, μ_B is Bohr magneton, g is the g factor, and we used the expressions from Ref. 33 up to the third order in temperature. The calculated exchange couplings (Table I) are in reasonable agreement with the experimental data down to 150 K (Fig. 4). The deviations at lower temperatures are likely related to the divergence of the HTSE at $T \leqslant J$. To improve the fit at higher temperatures, a slight adjustment of the exchange couplings is required. However, the third-order HTSE contains two J-dependent

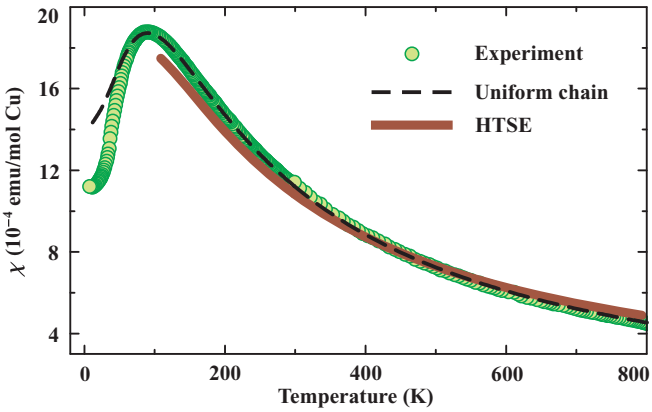

FIG. 4. (Color online) Fit of the experimental magnetic susceptibility data with the uniform chain model (dashed line) and the comparison to the HTSE of Eq. (2) (solid line). Experimental data are from Ref. 23.

terms only; hence an unconstrained fit of three exchange parameters is impossible.

To access temperatures below 150 K, a simplification of the model is required. Since J exceeds $|J_1|$ and J_2, the spin lattice is, to a first approximation, a set of uniform spin chains along a'. The respective 1D model[33] fits the experimental magnetic susceptibility down to 70 K with $J = 140$ K and $g = 2.22$. A similar fit with $J = 135$ K has been given in Ref. 23. However, Yamada *et al.*[23] erroneously assign the spin chains to the structural chains (in their notation, J corresponds to J_1). Our DFT calculations show that the uniform spin chains run perpendicular to the structural chains, whereas J_1 is FM. Such an intricate situation is not uncommon for low-dimensional magnets; see Refs. 34 and 35 for similar examples.

Below 70 K, the 1D uniform chain model overestimates the magnetic susceptibility of Cu_2GeO_4. This feature indicates an onset of 2D spin correlations. In contrast to the uniform spin-$\frac{1}{2}$ chain having finite susceptibility at zero temperature, 2D and 3D systems usually develop a long-range order with vanishing susceptibility at low temperatures. The onset temperature of 2D spin correlations is a rough measure of interchain couplings. Indeed, the temperature of 70 K conforms to our estimates of $J_1 = -60$ K and $J_2 = 80$ K, the couplings between the uniform spin chains.

B. Coupled cluster method

The coupled cluster method (CCM) and its application to frustrated spin systems have been previously reviewed in several articles; see, e.g., Refs. 21,36–47. Therefore, we give only a brief illustration of the main relevant features of the method. For more general information on the methodology of the CCM, see, e.g., Refs. 40 and 48, and references therein.

The CCM is a universal quantum many-body method. The starting point for a CCM calculation is the choice of a normalized reference or model state $|\Phi\rangle$, together with a complete set of (mutually commuting) multiconfigurational creation operators $\{C_L^+\}$ and the corresponding set of their Hermitian adjoints $\{C_L\}$. The CCM parametrizations of the ket and bra ground states (GSs) are given by

$$\begin{aligned} |\Psi\rangle &= e^S|\Phi\rangle, \qquad S = \sum_{I\neq 0}\mathcal{S}_I C_I^+; \\ \langle\tilde{\Psi}| &= \langle\Phi|\tilde{S}e^{-S}, \qquad \tilde{S} = 1 + \sum_{I\neq 0}\tilde{\mathcal{S}}_I C_I. \end{aligned} \tag{3}$$

Using $\langle\Phi|C_I^+ = 0 = C_I|\Phi\rangle \;\; \forall I \neq 0$, $C_0^+ \equiv 1$, the commutation rules $[C_L^+, C_K^+] = 0 = [C_L, C_K]$, the orthonormality condition $\langle\Phi|C_I C_J^+|\Phi\rangle = \delta_{IJ}$, and completeness $\sum_I C_I^+|\Phi\rangle\langle\Phi|C_I = 1 = |\Phi\rangle\langle\Phi| + \sum_{I\neq 0} C_I^+|\Phi\rangle\langle\Phi|C_I$, we get a set of nonlinear and linear equations for the correlation coefficients $\mathcal{S}_I$ and $\tilde{\mathcal{S}}_I$, respectively. We choose a reference state corresponding to the classical state of the spin model, i.e., a noncollinear reference state with up-down Néel-type correlations along the a' direction (uniform J chains) and with spiral correlations along the b' direction (frustrated J_1-J_2 chains). The spiral correlations are characterized by a pitch angle γ, i.e., $|\Phi\rangle = |\Phi(\gamma)\rangle$. In the quantum model, the pitch angle is typically different from the corresponding classical value $\gamma_{\rm cl}$. Hence, we do not choose the classical result for the pitch angle and rather consider γ as a free parameter in the CCM calculation. The value of γ has to be determined by the minimization of the GS energy (in a certain CCM approximation, see below) given by $E(\gamma) = \langle\Phi(\gamma)|e^{-S}He^S|\Phi(\gamma)\rangle$, i.e., from the $dE/d\gamma|_{\gamma=\gamma_{\rm qu}} = 0$ condition.

In order to find an appropriate set of creation operators, it is convenient to perform a rotation of the local axes on each of the spins so that all spins in the reference state align with the negative z direction. This rotation by an appropriate local angle $\delta_{i,n} = \delta_{i,n}(\gamma)$ of the spin on the lattice site (i,n) is equivalent to the spin-operator transformation

$$\left.\begin{aligned} s_{i,n}^x &= \cos\delta_{i,n}\hat{s}_{i,n}^x + \sin\delta_{i,n}\hat{s}_{i,n}^z; \quad s_{i,n}^y = \hat{s}_{i,n}^y \\ s_{i,n}^z &= -\sin\delta_{i,n}\hat{s}_{i,n}^x + \cos\delta_{i,n}\hat{s}_{i,n}^z \end{aligned}\right\}. \tag{4}$$

The reference state and the corresponding creation operators C_L^+ are given by

$$|\hat{\Phi}\rangle = |\downarrow\downarrow\downarrow\downarrow\cdots\rangle; \; C_L^+ = \hat{s}_{i,n}^+, \hat{s}_{i,n}^+\hat{s}_{j,m}^+, \hat{s}_{i,n}^+\hat{s}_{j,m}^+\hat{s}_{k,l}^+, \ldots, \tag{5}$$

where the indices $(i,n),(j,m),(k,l),\ldots$ denote arbitrary lattice sites. This specified form of the creation operators C_L^+ and the corresponding reference state $|\hat{\Phi}\rangle$ immediately make clear that the general relations listed below Eq. (3) are fulfilled. In the rotated coordinate frame, the Heisenberg Hamiltonian acquires a dependence on the pitch angle γ (see Ref. 21 for more details).

The order parameter (sublattice magnetization) in the rotated coordinate frame is given by $m = -1/N\sum_{i,n}^N\langle\tilde{\Psi}|s_{i,n}^z|\Psi\rangle$. The only approximation of the CCM is the truncation of the expansion of the correlation operators S and $\tilde{S}$. We use the well-established LSUBn scheme, where all multispin correlations on the lattice with n or fewer contiguous sites are taken into account.

In contrast to Ref. 21, which is focused on the $J \leqslant |J_1|, J_2$ regime, we consider the case of $J > |J_1|, J_2$. We also evaluate LSUBn approximations of higher order, up to $n = 8$. In the highest order of approximation, LSUB8, we have 21 124 configurations, i.e., 21 124 coupled nonlinear

equations have to be solved numerically. Moreover, the minimum of $E(\gamma)$ has to be found numerically to determine the quantum pitch angle $\gamma_{\rm qu}$. For the numerical calculations, we use the program package CCCM by D. J. J. Farnell and J. Schulenburg.[49]

Since the LSUBn becomes exact for $n \to \infty$, the numerical result can be improved by extrapolating the "raw" LSUBn data to $n \to \infty$ using the expression $m_n = m_\infty + a/n + b/n^2$ (cf. Refs. 38,40,45, and 48).

C. Ground state

To find the classical ground state of the model given by Eq. (1), we write the magnetic energy per lattice site for an arbitrary 2D propagation vector $\mathbf{k} = (k_x, k_y)$:

$$E = \tfrac{1}{2}[J \cos k_x + J_1 \cos k_y + J_2 \cos(2k_y)], \qquad (6)$$

where the unit cell of the spin lattice is used.[50] The energy minimum is found at $\mathbf{k} = [\pi, \arccos(-\frac{J_1}{4J_2})]$, which corresponds to the AFM order along a' and the spiral order along b'. The classical pitch angle is $\gamma = \arccos(-\frac{J_1}{4J_2}) = 79.19^\circ$ and does not depend on J; hence the a' and b' directions of the spin lattice are fully decoupled. The ordering along a' is controlled by J, whereas the ordering along b' is controlled by the competing couplings J_1 and J_2. To check the validity of this result for the quantum case, we use the CCM method and Lanczos diagonalization.

In CCM, we reduce our exchange couplings (Table I) to $J_1 = -1$ and $J_2 = \frac{4}{3}$ and vary J (in Cu_2GeO_4, $J = \frac{13}{6}$). The CCM results for γ and m as a function of J are shown in Fig. 5. In contrast to the classical pitch angle $\gamma_{\rm cl}$, the pitch angle of the quantum system ($\gamma_{\rm qu}$) slightly depends on J. In Cu_2GeO_4, we find $\gamma_{\rm qu} = 83.9^\circ$, which is about 6% larger than the classical angle, but about 5% smaller than the quantum pitch angle for the isolated chain, i.e., at $J = 0$. The coupling J affects the dimensionality of the system and has a stronger effect on the sublattice magnetization (see Fig. 5). The extrapolated value m_∞ has a maximum at $J \simeq -1.17 J_1$. The calculated

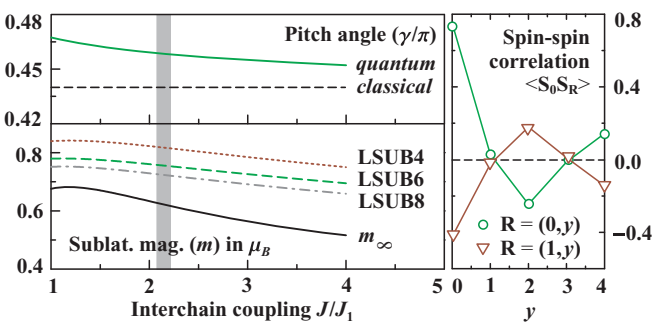

FIG. 5. (Color online) Left panel: The pitch angle (γ) and the sublattice magnetization (m) calculated by the CCM for $J_2 = \frac{4}{3}|J_1|$. The shaded bar shows the coupling regime of Cu_2GeO_4. Note that the quantum pitch angles $\gamma_{\rm qu}$ for the LSUBn approximations with $n = 4$, 6, and 8 almost coincide. Therefore, the shown LSUB8 curve represents effectively the limit $n \to \infty$. Right panel: Spin-spin correlation $\langle \mathbf{S}_0 \mathbf{S}_\mathbf{R} \rangle$, $\mathbf{R} = (x, y)$ along the J_1-J_2 chains (b' axis) for a finite system of $N = 32 = 4 \times 8$ sites at $J_2 = \frac{4}{3}|J_1|$ and $J = \frac{13}{6}|J_1|$.

exchange couplings in Cu_2GeO_4 lead to $m_\infty \sim 0.310$ (i.e., 0.62 μ_B).

The CCM results are confirmed by the Lanczos diagonalization data for the spin-spin correlation functions $\langle \mathbf{S}_0 \mathbf{S}_\mathbf{R} \rangle$ shown in the right panel of Fig. 5. We use a finite lattice comprising four 8-spin J_1-J_2 chains coupled by J. The correlations between nearest neighbors within the frustrated J_1-J_2 chains [$\mathbf{R} = (0,1)$] are close to zero, whereas the second-neighbor correlations [$\mathbf{R} = (0,2)$] are AFM. This conforms to the spiral ordering with the pitch angle close to 90° (neighboring spins are nearly orthogonal). The correlations between the structural chains [at $\mathbf{R} = (1, y)$] follow the intrachain correlations, yet showing the opposite sign. Thus, the ordering along a' is AFM.

D. Long-range order

The 2D model given by Eq. (1) is ordered at zero temperature only. To account for the actual long-range order in Cu_2GeO_4 below $T_N = 33$ K, the interlayer coupling J_c should be considered. The FM coupling J_c is compatible with J_1, yet competing with J and J_2. Assuming a similar ground state with the 2D propagation vector, we find that J_c modifies the energy in Eq. (6) by

$$\Delta E_{\rm 3D} = \frac{J_c}{2} \cos \frac{k_x}{4} \cos \frac{k_y}{2}. \qquad (7)$$

Using DFT estimates of individual exchange couplings (Table I), we arrive at the classical pitch angle modified by 0.15%: 79.07° vs 79.19° for the purely 2D model. The classical energy per lattice site is reduced by 0.5% (about 0.6 K). This simplified analysis shows that the interlayer coupling J_c is capable of stabilizing the 3D order in Cu_2GeO_4. However, the classical model does not reflect all the features of the real quantum model that, unfortunately, remains unfeasible for an accurate numerical study. In particular, the ordering temperature T_N cannot be determined with sufficient accuracy.

IV. DISCUSSION AND SUMMARY

Although not obvious at first glance, the microscopic magnetic model of Cu_2GeO_4 can be deduced from simple qualitative arguments. While the naive geometrical analysis of the crystal structure suggests a 3D pyrochlore-lattice magnetism, a closer look at the crystal structure identifies 2D features. In most of the Cu^{2+} oxides, electronic structure and magnetism are controlled by the arrangement of CuO_4 plaquettes, which are the basic structural entities. Chains of edge-sharing plaquettes give rise to frustrated J_1-J_2 spin chains,[9–12] yet the coplanar arrangement of the plaquettes in the neighboring structural chains induces a strong AFM coupling along a'. Overall, we find magnetic layers in the ab plane, along with a weak FM interlayer coupling J_c. By combining the frustration along b' with the strong unfrustrated exchange along a', Cu_2GeO_4 expands the family of cuprates featuring frustrated spin chains.

The dearth of the experimental data and the complexity of the 2D frustrated J-J_1-J_2 lattice restrict the opportunities for an experimental verification of our microscopic model.

Nevertheless, the tangible success of DFT in unraveling complex spin lattices for a range of transition-metal compounds[27,35,51,52] is a solid justification of our results. The 2D nature of the system and the frustrated couplings along b' are confirmed by qualitative arguments and by a reference to similar Cu^{2+} compounds (see Sec. II). Further on, numerical estimates of individual exchanges conform to the experimental magnetic susceptibility (Sec. III A). An ultimate test of the proposed model requires a study of the ground state by neutron or resonant x-ray scattering. Presently, we note that our model does predict the long-range magnetic order, in contrast to the strongly anisotropic pyrochlore lattice that might have a quantum-disordered valence-bond-solid[24] or a gapless spin-liquid[53] ground state.

The experimental data for Cu_2GeO_4 and accurate theoretical results for the ground state disclose the basic features of our model. At high temperatures, thermodynamic properties are guided by the uniform spin chains along a'. The apparent spin-chain behavior is likely related to the partial cancelation of FM J_1 and AFM J_2 in the second-order term for the susceptibility [see Eq. (2)]. A further evidence is the perfect fit of the experimental magnetic susceptibility down to 70 K ($T/J \simeq 0.5$). The frustrated couplings along b' come into play at lower temperatures and essentially determine the ground state. The leading exchange J drives AFM ordering along a'. The ordering along b' has to satisfy the frustrated couplings J_1 and J_2 and is, therefore, a spiral, similar to a single J_1-J_2 frustrated spin chain. The interlayer coupling J_c should stabilize the long-range order up to T_N without changing the basic features of the ground state: the collinear AFM order along a' and the spiral order along b'.

The highly accurate CCM approach provides reliable information on the ground state of the 2D system. We find a pitch angle of $\gamma \simeq 84^\circ$ and a sublattice magnetization close to 0.62 μ_B. Both γ and m are renormalized with respect to the classical values and suggest strong quantum fluctuations in the system. Enhanced quantum fluctuations should be ascribed to the reduced dimensionality and frustration. The magnetic ordering temperature $T_N/J \simeq 0.25$ is also suggestive of strong quantum fluctuations. For example, a quasi-2D system of square lattices with a weak interlayer coupling $J_\perp/J = 0.01$ (compare to $|J_c|/J \simeq 0.01$) orders at a higher temperature of $T_N/J \simeq 0.33$ (Ref. 54). The quantum effects in the system could be further probed by an experimental study of the ground state.

An interesting feature of the spiral magnetic order is the possible emergence of electric polarization strongly coupled to the magnetism.[6] The direction of the electric polarization depends on the twisting direction of the spiral. In Cu_2GeO_4, the AFM coupling J leads to opposite twisting directions in the neighboring spirals; hence the polarization is canceled. However, the proposed antiferroelectricity of Cu_2GeO_4 does not preclude the strong magnetoelectric coupling and should stimulate further experimental investigation of the compound. We also note that the family of 2D frustrated materials representing the J-J_1-J_2 model can be further expanded by CuNCN lying in the limit of $J \gg |J_1|, J_2$.[13]

In summary, we have shown that the electronic structure of Cu_2GeO_4 contradicts the previous, empirical-based spin model of the anisotropic pyrochlore lattice. The comprehensive computational study discloses the quasi-2D nature of this compound and suggests an original 2D spin model comprising frustrated and uniform spin chains along the two dimensions. Theoretical results for this model show the robust nature of the spiral ground state that is subject to strong quantum effects, evidenced by the reduced sublattice magnetization of 0.62 μ_B and the renormalized pitch angle of about 84°.

ACKNOWLEDGMENTS

We are grateful to Oleg Janson and Deepa Kasinathan for fruitful discussions and careful reading of the manuscript. A. T. acknowledges financial support from the Alexander von Humboldt Foundation. J. R. appreciates the funding by the DFG (Project RI 615/16-1).

*altsirlin@gmail.com
†Helge.Rosner@cpfs.mpg.de

[1] H. T. Diep, eds., *Frustrated Spin Systems* (World Scientific, Singapore, 2004).
[2] U. Schollwöck, J. Richter, D. J. J. Farnell, and R. F. Bishop, eds., *Quantum Magnetism* (Springer, New York, 2004).
[3] A. V. Sologubenko, T. Lorenz, H. R. Ott, and A. Freimuth, J. Low Temp. Phys. **147**, 387 (2007).
[4] M. E. Zhitomirsky and A. Honecker, J. Stat. Mech. (2004) P07012.
[5] J. Schnack, R. Schmidt, and J. Richter, Phys. Rev. B **76**, 054413 (2007).
[6] S.-W. Cheong and M. Mostovoy, Nat. Mater. **6**, 13 (2007).
[7] S. Furukawa, M. Sato, and S. Onoda, Phys. Rev. Lett. **105**, 257205 (2010).
[8] V. V. Mazurenko, S. L. Skornyakov, A. V. Kozhevnikov, F. Mila, and V. I. Anisimov, Phys. Rev. B **75**, 224408 (2007), and references therein.
[9] A. A. Gippius, E. N. Morozova, A. S. Moskvin, A. V. Zalessky, A. A. Bush, M. Baenitz, H. Rosner, and S.-L. Drechsler, Phys. Rev. B **70**, 020406(R) (2004); T. Masuda, A. Zheludev, B. Roessli, A. Bush, M. Markina, and A. Vasiliev, *ibid.* **72**, 014405 (2005).
[10] M. Enderle, C. Mukherjee, B. Fåk, R. K. Kremer, J.-M. Broto, H. Rosner, S.-L. Drechsler, J. Richter, J. Malek, A. Prokofiev, W. Assmus, S. Pujol, J.-L. Raggazzoni, H. Rakoto, M. Rheinstädter, and H. M. Rønnow, Europhys. Lett. **70**, 237 (2005); S.-L. Drechsler, S. Nishimoto, R. Kuzian, J. Málek, J. Richter, J. van den Brink, M. Schmitt, and H. Rosner, e-print arXiv:1006.5070; M. Enderle, B. Fåk, H.-J. Mikeska, R. K. Kremer, A. Prokofiev, and W. Assmus, Phys. Rev. Lett. **104**, 237207 (2010).
[11] L. Capogna, M. Mayr, P. Horsch, M. Raichle, R. K. Kremer, M. Sofin, A. Maljuk, M. Jansen, and B. Keimer, Phys. Rev. B **71**, 140402(R) (2005); S.-L. Drechsler, J. Richter, A. A. Gippius, A. Vasiliev, A. A. Bush, A. S. Moskvin, J. Málek, Y. Prots, W. Schnelle, and H. Rosner, Europhys. Lett. **73**, 83 (2006).

[12]M. Schmitt, O. Janson, M. Schmidt, S. Hoffmann, W. Schnelle, S.-L. Drechsler, and H. Rosner, Phys. Rev. B **79**, 245119 (2009); M. G. Banks, R. K. Kremer, C. Hoch, A. Simon, B. Ouladdiaf, J.-M. Broto, H. Rakoto, C. Lee, and M.-H. Whangbo, *ibid.* **80**, 024404 (2009).

[13]A. A. Tsirlin and H. Rosner, Phys. Rev. B **81**, 024424 (2010).

[14]S. Park, Y. J. Choi, C. L. Zhang, and S.-W. Cheong, Phys. Rev. Lett. **98**, 057601 (2007); Y. Naito, K. Sato, Y. Yasui, Y. Kobayashi, Y. Kobayashi, and M. Sato, J. Phys. Soc. Jpn. **76**, 023708 (2007); S. Seki, T. Kurumaji, S. Ishiwata, H. Matsui, H. Murakawa, Y. Tokunaga, Y. Kaneko, T. Hasegawa, and Y. Tokura, Phys. Rev. B **82**, 064424 (2010).

[15]A. S. Moskvin, Y. D. Panov, and S.-L. Drechsler, Phys. Rev. B **79**, 104112 (2009); A. S. Moskvin and S.-L. Drechsler, Europhys. Lett. **81**, 57004 (2008).

[16]I. Affleck, M. P. Gelfand, and R. R. P. Singh, J. Phys. A **27**, 7313 (1994).

[17]A. W. Sandvik, Phys. Rev. Lett. **83**, 3069 (1999).

[18]N. Laflorencie and D. Poilblanc, Phys. Rev. Lett. **90**, 157202 (2003).

[19]H. T. Ueda and K. Totsuka, Phys. Rev. B **80**, 014417 (2009); M. E. Zhitomirsky and H. Tsunetsugu, Europhys. Lett. **92**, 37001 (2010).

[20]S. Nishimoto, S.-L. Drechsler, R. Kuzian, J. van der Brink, and J. Richter, e-print arXiv:1005.5500.

[21]R. Zinke, S.-L. Drechsler, and J. Richter, Phys. Rev. B **79**, 094425 (2009).

[22]W. Hegenbart, F. Rau, and K.-J. Range, Mater. Res. Bull. **16**, 413 (1981).

[23]T. Yamada, Z. Hiroi, M. Takano, M. Nohara, and H. Takagi, J. Phys. Soc. Jpn. **69**, 1477 (2000).

[24]O. A. Starykh, A. Furusaki, and L. Balents, Phys. Rev. B **72**, 094416 (2005).

[25]K. Koepernik and H. Eschrig, Phys. Rev. B **59**, 1743 (1999).

[26]J. P. Perdew and Y. Wang, Phys. Rev. B **45**, 13244 (1992).

[27]O. Janson, A. A. Tsirlin, M. Schmitt, and H. Rosner, Phys. Rev. B **82**, 014424 (2010).

[28]A. A. Tsirlin, O. Janson, and H. Rosner, Phys. Rev. B **82**, 144416 (2010).

[29]O. Janson, W. Schnelle, M. Schmidt, Y. Prots, S.-L. Drechsler, S. K. Filatov, and H. Rosner, New J. Phys. **11**, 113034 (2009).

[30]O. Janson, J. Richter, P. Sindzingre, and H. Rosner, Phys. Rev. B **82**, 104434 (2010).

[31]H. Eschrig and K. Koepernik, Phys. Rev. B **80**, 104503 (2009).

[32]The symmetry of the model restricts the computationally feasible size of the finite lattice to 4×4, with two J_2 bonds only.

[33]D. C. Johnston, R. K. Kremer, M. Troyer, X. Wang, A. Klümper, S. L. Bud'ko, A. F. Panchula, and P. C. Canfield, Phys. Rev. B **61**, 9558 (2000).

[34]A. W. Garrett, S. E. Nagler, D. A. Tennant, B. C. Sales, and T. Barnes, Phys. Rev. Lett. **79**, 745 (1997).

[35]E. E. Kaul, H. Rosner, V. Yushankhai, J. Sichelschmidt, R. V. Shpanchenko, and C. Geibel, Phys. Rev. B **67**, 174417 (2003); A. A. Tsirlin and H. Rosner, *ibid.* **83**, 064415 (2011).

[36]R. Bursill, G. A. Gehring, D. J. J. Farnell, J. B. Parkinson, T. Xiang, and C. Zeng, J. Phys. Condens. Matter **7**, 8605 (1995).

[37]R. F. Bishop, D. J. J. Farnell, and J. B. Parkinson, Phys. Rev. B **58**, 6394 (1998).

[38]S. E. Krüger, J. Richter, J. Schulenburg, D. J. J. Farnell, and R. F. Bishop, Phys. Rev. B **61**, 14607 (2000).

[39]S. E. Krüger and J. Richter, Phys. Rev. B **64**, 024433 (2001).

[40]D. J. J. Farnell and R. F. Bishop, Lect. Notes Phys. **645**, 307 (2004).

[41]R. Darradi, J. Richter, and D. J. J. Farnell, Phys. Rev. B **72**, 104425 (2005).

[42]D. Schmalfuß, R. Darradi, J. Richter, J. Schulenburg, and D. Ihle, Phys. Rev. Lett. **97**, 157201 (2006).

[43]R. Darradi, O. Derzhko, R. Zinke, J. Schulenburg, S. E. Krüger, and J. Richter, Phys. Rev. B **78**, 214415 (2008).

[44]R. F. Bishop, P. H. Y. Li, R. Darradi, and J. Richter, J. Phys. Condens. Matter **20**, 255251 (2008).

[45]R. F. Bishop, P. H. Y. Li, D. J. J. Farnell, and C. E. Campbell, Phys. Rev. B **79**, 174405 (2009).

[46]J. Richter, R. Darradi, J. Schulenburg, D. J. J. Farnell, and H. Rosner, Phys. Rev. B **81**, 174429 (2010).

[47]R. Zinke, J. Richter, and S.-L. Drechsler, J. Phys. Condens. Matter **22**, 446002 (2010).

[48]R. F. Bishop, D. J. J. Farnell, S. E. Krüger, J. B. Parkinson, J. Richter, and C. Zeng, J. Phys. Condens. Matter **12**, 6887 (2000).

[49]See [http://www-e.uni-magdeburg.de/jschulen/ccm/index.html].

[50]The b' parameter of the spin lattice is twice smaller than the crystallographic lattice parameter in the ab plane.

[51]R. Valenti, T. Saha-Dasgupta, C. Gros, and H. Rosner, Phys. Rev. B **67**, 245110 (2003).

[52]A. A. Tsirlin and H. Rosner, Phys. Rev. B **82**, 060409(R) (2010).

[53]P. Sindzingre, J.-B. Fouet, and C. Lhuillier, Phys. Rev. B **66**, 174424 (2002).

[54]C. Yasuda, S. Todo, K. Hukushima, F. Alet, M. Keller, M. Troyer, and H. Takayama, Phys. Rev. Lett. **94**, 217201 (2005).